Doklady Earth Sciences, Vol. 372, No. 4, 2000, pp. 690–694. Translated from Doklady Akademii Nauk, Vol. 372, No. 1, 2000, pp. 108–112.

GEOPHYSICS

An Effective Model of the Layered Elastic-Porous Medium

L. A. Molotkov and A. V. Bakulin

Presented by Academician S.V. Gol'din October 1, 1998

Received November 12, 1998

The present development of the theory of seismic propagation, technique of seismic measurements, and computer technologies has aroused considerable interest in the propagation of waves within porous and fissured media. Natural oil and gas reservoirs belong to such media. The theoretical study of wave processes in the media is accomplished on the basis of effective models. The averaging of periodic layered media is one of the methods for constructing effective models of porous and fissured media. The averaging of alternating elastic and liquid layers was performed in [1, 2], whereas the averaging of structures, in which porous Biot layers alternate with other porous layers or with elastic or liquid layers, was performed in [8].

The present work is devoted to investigating an effective model of the layered elastic-porous medium. This model is applicable to the description of rocks and materials, in which the liquid flow is possible only in a certain direction. This often takes place in natural conditions with the presence of a system of cracks. The types of waves propagating in the specified model are studied, their velocities are determined, possible variants of all wave fronts and their specific features are identified.

1. EQUATIONS OF THE EFFECTIVE MODEL

Suppose that a periodic medium $0 \le z \le H$ consisting of n periods is specified. Each period has the thickness h and contains layer 1 of the porous medium, described by the model of Biot [4], and elastic layer 2 with the thicknesses $h_1 = \theta_1 h$ and $h_2 = \theta_2 h$ ($\theta_1 + \theta_2 = 1$). The following conditions are fulfilled at the boundary between the layers:

$$U_{x1} = U_{x2}, \quad U_{z1} = U_{z2}, \quad W_{z1} = 0, \qquad \tau_{zz1} = \tau_{zz2}, \quad \tau_{xz1} = \tau_{xz2}, \tag{1.1}$$

Steklov Mathematical Institute, St. Petersburg Division (POMI), Russian Academy of Sciences, ul. Fontanka 27, St. Petersburg, 191011 Russia

St. Petersburg State University, Universitetskaya nab., St. Petersburg, 199164 Russia

where U_{x1} and U_{z1} are the displacements in the solid phase of the porous layer, U_{x2} and U_{z2} are the displacements in the elastic layer, W_z is the relative displacement of the liquid phase of the porous layer along the z axis, z, τ_{xz1} and τ_{zz1} are the total stresses in the porous layer, and τ_{xz2} and τ_{zz2} are the stresses in the elastic layer. Indices 1 and 2 in conditions (1.1) denote the numbers of layers.

The following equations of the effective model were derived for this medium in [3]:

$$\begin{aligned}
\tau_{xx} &= P\frac{\partial U_x}{\partial x} + F\frac{\partial U_z}{\partial z} + M\frac{\partial W_x}{\partial x},\\
\tau_{zz} &= F\frac{\partial U_x}{\partial x} + C\frac{\partial U_z}{\partial z} + Q\frac{\partial W_x}{\partial x},\\
-p &= M\frac{\partial U_x}{\partial x} + Q\frac{\partial U_z}{\partial z} + R\frac{\partial W_x}{\partial x},\\
\tau_{xz} &= L\left(\frac{\partial U_x}{\partial z} + \frac{\partial U_z}{\partial x}\right);
\end{aligned} \tag{1.2}$$

$$\begin{aligned}
\frac{\partial \tau_{xx}}{\partial x} + \frac{\partial \tau_{xz}}{\partial z} &= \rho\frac{\partial^2 U_x}{\partial t^2} + \rho_f\frac{\partial^2 W_x}{\partial t^2},\\
-\frac{\partial p}{\partial x} &= \rho_f\frac{\partial^2 U_x}{\partial t^2} + m_x\frac{\partial^2 W_x}{\partial t^2},\\
\frac{\partial \tau_{xz}}{\partial x} + \frac{\partial \tau_{zz}}{\partial z} &= \rho\frac{\partial^2 U_z}{\partial t^2},
\end{aligned} \tag{1.3}$$

where p is the pressure in the liquid phase, ρ is the average density of the medium, ρ_f is the average density of the liquid phase, and m_x characterizes the sinuosity of the pore space along the x axis [4]. Expressions for the coefficients in equations (1.2) and (1.3) through the parameters of both layers are presented in [3].

The medium described by equations (1.2) and (1.3) is a particular case of the Biot transversal-isotropic model, in which

$$m_z = \infty, \quad W_z = 0. \tag{1.4}$$

For subsequent investigation of this medium, it will be useful to substitute the Hooke law equations (1.2) into the continuum equations (1.3) and obtain the Lame equations for the considered effective model:

$$\begin{aligned}
&\left(P\frac{\partial^2}{\partial x^2}+L\frac{\partial^2}{\partial z^2}-\rho\frac{\partial^2}{\partial t^2}\right)U_x+(F+L)\frac{\partial^2 U_z}{\partial x\partial z}\\
&\quad+\left(M\frac{\partial^2}{\partial x^2}-\rho_f\frac{\partial^2}{\partial t^2}\right)W_x=0,\\
&(F+L)\frac{\partial^2 U_x}{\partial x\partial z}+\left(L\frac{\partial^2}{\partial x^2}+C\frac{\partial^2}{\partial z^2}-\rho\frac{\partial^2}{\partial t^2}\right)U_z\\
&\quad+Q\frac{\partial^2 W_x}{\partial x\partial z}=0,\\
&\left(M\frac{\partial^2}{\partial x^2}-\rho_f\frac{\partial^2}{\partial t^2}\right)U_x+Q\frac{\partial^2 U_z}{\partial x\partial z}\\
&\quad-\left(R\frac{\partial^2}{\partial x^2}-m_x\frac{\partial^2}{\partial t^2}\right)W_x=0.
\end{aligned}\tag{1.5}$$

2. THE CHARACTERISTIC FUNCTION $\alpha(\tau)$

Solutions of equations (1.5) can be expressed in the form of integrals of the Fourier integral type representing the superposition of flat waves

$$e^{ik(\tau t-x-\alpha z)},\tag{2.1}$$

in this case

$$\tau=\frac{v_{ph}}{\sin\varphi},\qquad \alpha=\cot\varphi,\tag{2.2}$$

where v_{ph} is the phase velocity, φ is the angle between the normal to the flat front and the z axis, and k is the component of the wave vector along the x axis. Characteristic features of these integral transformations coincide with wave fronts and are determined by the real-valued function $\alpha(\tau)$. In the case of a point source located at the origin, the fronts are expressed by the following parametric equalities [5]:

$$x=t\left(\frac{\tau-\alpha(\tau)}{\alpha'(\tau)}\right),\qquad z=\frac{t}{\alpha'(\tau)},\tag{2.3}$$

where $\alpha=\cot\varphi$ and φ is the angle between the normal to the front and the z axis.

In order to find the function $\alpha(\tau)$, it is necessary in accordance with expressions (2.1), to accomplish the substitution

$$\frac{\partial}{\partial x}\sim 1,\qquad \frac{\partial}{\partial z}\sim\alpha,\qquad \frac{\partial}{\partial t}\sim-\tau.\tag{2.4}$$

After this substitution, the condition of the simultaneity of equations (2.1) will be expressed by the equality

$$\begin{vmatrix}
P+L\alpha^2-\rho\tau^2 & (F+L)\alpha & M-\rho_f\tau^2\\
(F+L)\alpha & L+C\alpha^2-\rho\tau^2 & Q\alpha\\
M-\rho_f\tau^2 & Q\alpha & R-m_x\tau^2
\end{vmatrix}=0,\tag{2.5}$$

which is analogous to the Cristoffel equation. As a result of the determinant calculation, relationship (2.5) will be substituted by a certain biquadratic equation, whose solution will provide an analytical representation for the function $\alpha(\tau)$.

Let us specify a number of properties of this function and its plots. The function $\alpha(\tau)$ has the roots $\tau = v_{1,2,3}$ and the pole $\tau = v_7$ that can be represented by the following equalities:

$$v_{1,2}^2=\frac{R\rho+Pm_x-2M\rho_f\pm\sqrt{(R\rho+Pm_x-2M\rho_f)^2-4(PR-M^2)(\rho m_x-\rho_f^2)}}{2(\rho m_x-\rho_f^2)},\tag{2.6}$$

$$v_3^2=\frac{L}{\rho},\qquad v_7^2=\frac{CR-Q^2}{m_xC}.\tag{2.7}$$

At large τ and α the branches of the plots have two asymptotes

$$\alpha=\frac{\tau}{v_4},\qquad \alpha=\frac{\tau}{v_6},\tag{2.8}$$

$$v_4^2=\frac{C}{\rho},\qquad v_6^2=\frac{Lm_x}{\rho m_x-\rho_f^2}.\tag{2.9}$$

The function $\alpha(\tau)$ has no extremums, but its derivatives can change signs at the turning points, where $\alpha'(\tau)=\infty$.

The plots of the function $\alpha(\tau)$ are symmetrical with respect to the coordinate axes.

Based on formulas (2.5), (2.7), one can specify the initial and end points for the three branches of plots of the function $\alpha(\tau)$ in the region $\tau > 0$, $\alpha > 0$. Having connected their points into smooth curves, we shall obtain the approximate position of these branches. Figures 1–3 portray the plots of the functions $\alpha(\tau)$ for three cases of relationships between velocities:

$$\begin{aligned}
&1)\ v_1>v_7>v_{2,3}>v_{3,2},\\
&2)\ v_1>v_{2,3}>v_7>v_{3,2},\\
&3)\ v_1>v_{2,3}>v_{3,2}>v_7,
\end{aligned}\tag{2.10}$$

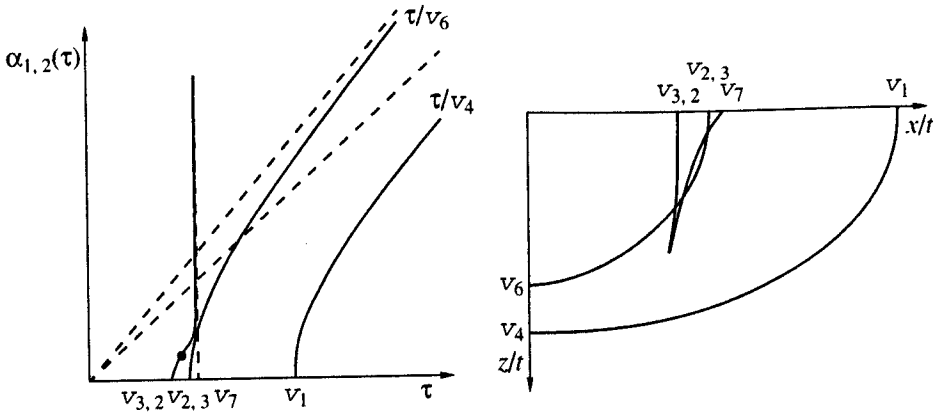

Fig. 1.

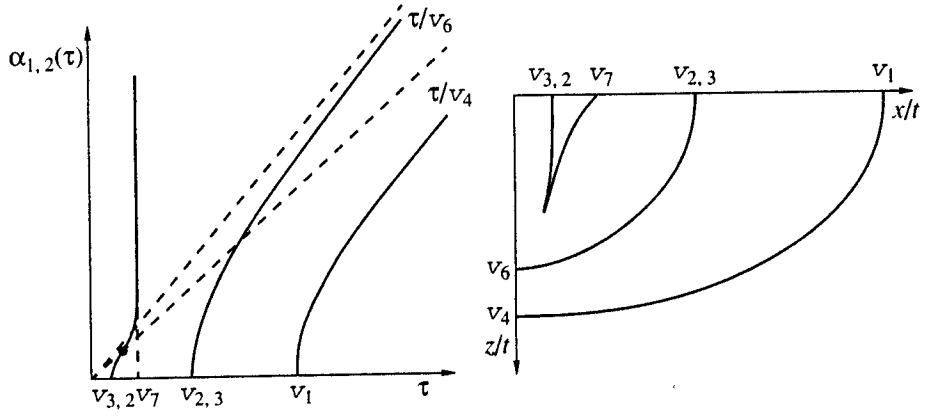

Fig. 2.

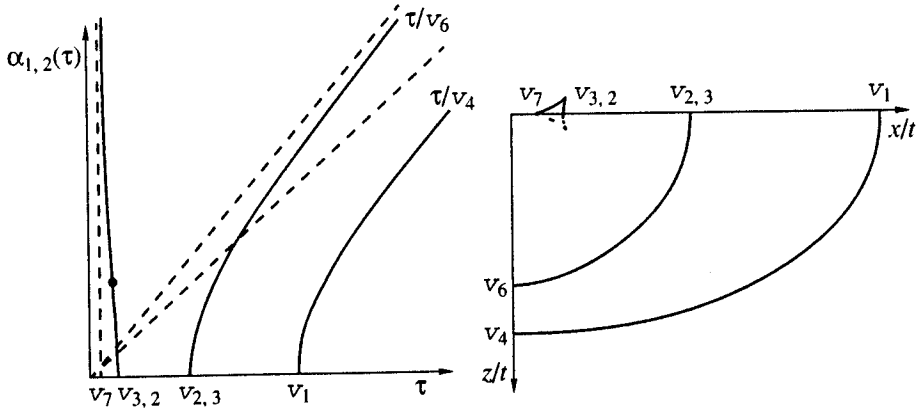

Fig. 3.

where $v_{2,3} = \max(v_2, v_3)$ and $v_{3,2} = \min(v_2, v_3)$. Let us refer to the branches issuing from the points $(v_1, 0)$, $(v_2, 0)$, and $(v_3, 0)$ as the first, second, and third branches. The plots depicted in Figs. 1–3 do not contain any turning points and on the third branch contain only a single inflection point ($\alpha''(\tau) = 0$) marked by a bolded dot. In a general consideration, it is necessary to take into account possible turning points and additional inflection points. However, the number of these points is restricted by the condition stating that a straight line cannot intersect the plots of the function $\alpha(\tau)$ throughout the entire plane τ, α more than six times, whereas the straight line parallel to the α axis can intersect these plots no more than four times. This particularly follows from the specified restrictions that the first branch does not contain any inflection or turning points. The analogous restrictions were also established for the curves of refraction (slowness).

3. WAVE FRONTS FROM THE POINT SOURCE

According to formulas (2.3), three wave fronts excited by the point source located at the plat origin correspond to the three branches of the $\alpha(\tau)$ function plot. These fronts are shown in Figs. 1–3 next to the corresponding $\alpha(\tau)$ plots. The forefront propagates along the x and z axes at the velocities v_1 and v_4. Since there are no special points on the first branch, the forefront is always convex and corresponds to the first (fast) longitudinal wave. We shall begin the investigation of two remaining fronts from the case, when the second and third branches do not contain any turning points or additional inflection points. The second front velocities along the x and z axes are equal to $v_{2,3}$ and v_6. In this case, v_3 and v_6 are the propagation velocities of transverse waves, whereas v_2 is the velocity of the second (slow) longitudinal wave [4], in which the skeleton and fluid displacements occur in the antiphase. The second longitudinal wave cannot propagate along the z axis due to condition (1.4). Therefore, the third front has a triangular shape in the quadrant $x > 0$, $z > 0$ and propagates only along the x axis. This front intersects the x axis at one point and touches this axis at another point. The specified points move at the velocities $v_{3,2}$ and v_7. The angular point corresponding to the inflection point indicated in Figs. 1–3 lies on the third front.

Let us now dwell on the cases, when turning points and additional inflection points are located on the second and third branches of the plot. The angular point on the front corresponds to each inflection point. Since the number of additional inflection points is equal to 2 or 4, simple or double loops [6] are formed between the relevant angular points on the front inside the quadrant $x > 0$, $z > 0$ (Fig. 4). The turning points on the branches can be located near their beginnings and asymptotes. In the first case, the front forms a protrusion into the quadrant $x > 0$, $z < 0$, and in the second case, the front protrudes into the quadrant $x < 0$, $z > 0$. The fronts corresponding to these conditions are shown in Fig. 4. In both cases, angular points on the front correspond to turning points, the front intersects the axes at an oblique angle, and both of the protrusions (with due regard for the symmetry of the plots) form loops located along the axes. For brevity, these complicated cases are illustrated in Fig. 4 only for the second front.

Note that the velocities v_1, v_2, and v_6 coincide with the velocities of waves propagating along the axes within the Biot transversal-isotropic medium. The expressions for velocities v_3 and v_6 can be obtained from the relevant expressions for velocities in the specified medium after the limiting transition $m_z \to \infty$. Velocity v_7 is a special one. Special investigations have shown that the symmetrical wave in a thin isolated Biot layer, at the boundaries of which the conditions $U_x = 0$, $W_z = 0$, and $\tau_{zz} = 0$ are fulfilled, also propagates at this velocity.

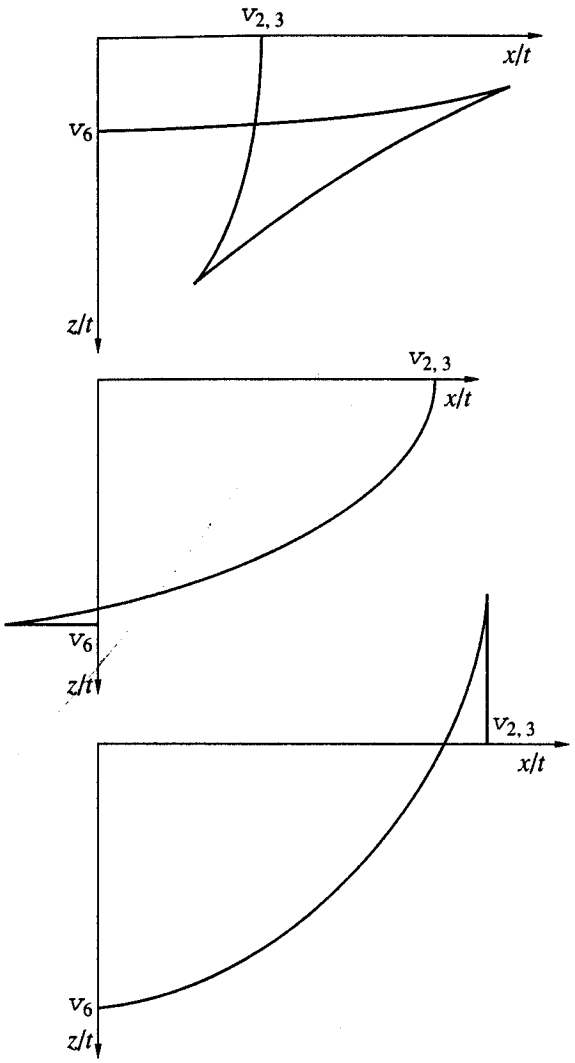

Fig. 4.

4. CASES WHEN THE THICKNESS OF ONE OF THE LAYERS EXCEEDS BY FAR THAT OF THE OTHER LAYER

Let us first consider the case, when the inequality

$$\theta_2 \ll 1. \tag{4.1}$$

is fulfilled for a relative thickness of the elastic layers θ_2 in the initial periodic medium. Using explicit expressions for the coefficients appearing in equations (1.2) and (1.3) [3], we arrive at the conclusion that under condition (4.1) these coefficients are approximately equal to the relevant parameters of Biot layers. In this case, equalities (1.4) are fulfilled. Therefore, the effective model of the porous medium crosscut by solid impermeable partitions is a particular case of the Biot transversal-isotropic medium, where $m_z = \infty$. This medium is also described by equations (1.2) and (1.3). In the zero-order approximation, parameters of porous

layers of the initial medium can be taken as parameters for these equations.

In the case, when

$$\theta_1 \ll 1, \tag{4.2}$$

explicit expressions for the coefficients entering into equations (1.2) and (1.3) are transformed into the relationships

$$P = C = \lambda_2 + 2\mu_2, \quad F = \lambda_2, \quad L = \mu_2,$$
$$R = \frac{R_1 C_1 - Q_1^2}{\theta_1 C_1}, \quad \rho = \rho_2, \tag{4.3}$$
$$\rho_f = \theta_1 \rho_{f1}, \quad m_x = \frac{m_{x1}}{\theta_1},$$

where C_1, R_1, Q_1, ρ_{f1}, and m_{x1} are the parameters of porous layer 1 and λ_2, μ_2, and ρ_2 are the parameters of elastic layer 2. It follows from equalities (4.3) that at the indefinite diminishing of θ_1, the R and m_x values indefinitely grow, which results in the fact that the second equation (1.2) and the third equation (1.3) lose their meaning, $W_x = 0$, and the remaining equations (1.2) and (1.3) become the equations of the homogeneous isotropic elastic medium. Taking into account inequality (4.2) and relationships (4.3), expressions for velocities (2.7), (2.8), and (2.10) can be substituted by the formulas

$$v_1^2 = v_4^2 = \frac{\lambda_2 + 2\mu_2}{\rho_2}, \quad v_3^2 = v_6^2 = \frac{\mu_2}{\rho_2},$$
$$v_2^2 = v_7^2 = \frac{R_1 C_1 - Q_1^2}{C_1 m_x}, \tag{4.4}$$

from which it follows that the triangular front at $\theta_1 \to 0$ narrows down to a point, whereas the forefront and the second front are transformed into the fronts of longitudinal and transverse waves.

ACKNOWLEDGMENTS

This work was supported by the Russian Foundation for Basic Research, project no. 96-05-66207.

REFERENCES

1. Molotkov, L.A., *Zap. Nauch. Sem. LOMI*, 1979, vol. 89, pp. 219–233.
2. Schoenberg, M., *Wave Motion*, 1984, vol. 6, pp. 303–320.
3. Molotkov, L.A. and Bakulin, A.V., *Zap. Nauch. Sem. POMI*, 1997, vol. 239, pp. 140–163.
4. Biot, M.A., *J. Appl. Phys.*, 1962, vol. 33, no. 4, pp. 1482–1498.
5. Molotkov, L.A. and Khilo, A.E., *Zap. Nauch. Sem. LOMI*, 1983, vol. 140, pp. 105–122.
6. Molotkov, L.A. and Bakulin, A.V., *Zap. Nauch. Sem. POMI*, 1995, vol. 230, pp. 172–195.

Doklady Earth Sciences, Vol. 372, No. 4, 2000, pp. 695–697. Translated from Doklady Akademii Nauk, Vol. 372, No. 2, 2000, pp. 225–227.

GEOCHEMISTRY

Specific Features of ε_{Nd} Distribution in Riftogenic Igneous Rocks

E. A. Landa and B. A. Markovskii

Presented by Academician D.V. Rundqvist March 17, 1999

Received May 17, 1999

Modern geochemistry points out two principal trends in the chemical evolution of magma sources [15]. The first trend is referred to the compositional variation of primordial Earth after crust separation (evolution of depleted mantle sources). The second trend characterizes the evolution of the continental crust, which for the most part was created as early as the Archean. However, a great number of igneous rocks cannot be referred to either of the two above-mentioned evolutionary trends. In addition to the rocks from oceanic islands, and to some extent from the island arcs, this group includes riftogenic igneous rocks. In the ε_{Nd} *versus* geological time plot, which exhibits the specific features of deep-seated magma sources, the field of such rocks is almost completely plotted between the fields related to the rocks derived from crustal and depleted mantle sources. In addition, the relationship of ε_{Nd} *versus* the age and type of riftogenic structures is revealed. Several riftogenic igneous rock assemblages can be distinguished with respect to ε_{Nd} distribution (figure).

Early proterozoic igneous rock assemblages related to the riftogenic systems at ancient shields. In particular, they are represented by some rocks from the Kola–Karelian region where the location of riftogenic systems to a great extent is controlled by a position of Archean greenstone belts. The following sequence of spatially related structures is outlined: Archean greenstone belts—riftogenic belts of large peridotite–pyroxenite–gabbro–norite layered intrusions (2.5–2.4 Ga)—riftogenic volcanosedimentary basins (2.1–1.8 Ga). The variation of ε_{Nd} for respective rocks is coherent with this sequence (figure). In rocks from greenstone belts, the ε_{Nd} value corresponds to the model value of the depleted mantle. The transition to belts of layered intrusions is expressed in a contribution of an enriched (fertile) component with a return to the ε_{Nd} value close to the average model value for the Earth. In rocks from younger volcanosedimentary basins, the relative amount of the enriched component again diminishes and ε_{Nd} approaches a level typical of older greenstone belts, which, however, do not achieve the parameters of depleted mantle for that time. The isotope-geochemical evolution is combined with an evolution of other typical characteristics of magmatic assemblages. Basaltic and komatiitic magmas of greenstone belts gave way to the boninite-like magmas of layered intrusions, and then to picritic, ferropicritic, and ferrobasaltic magmas of volcanosedimentary basins. It should be emphasized that the variation of melt compositions, in particular, their lithophile affinity reveals a reverse correlation with ε_{Nd}.

Late proterozoic igneous rock assemblages in riftogenic systems of folded region–platforms transitional zones are, in particular, represented by rocks of the Olokit–Patom system with so-called paired ultramafic and mafic (Ti-bearing peridotite–pyroxenite–gabbro and Ni-bearing olivinite–troctolite–gabbro) intrusive associations close in composition but distinct in geochemical and metallogenic specialization [4]. This difference is combined with a contrast in isotope-geochemical characteristics. For example, the rocks of the Chai peridotite–pyroxenite–gabbro pluton, which is located on the slope of the Olokit riftogenic volcanosedimentary basin, are distinguished by positive ε_{Nd} values corresponding to the depleted mantle (figure). At the same time, the rocks of the Yoko–Dovyren olivine–troctolite–gabbro pluton residing in the same structure are characterized by anomalous negative ε_{Nd} values (figure) indicating a substantial contribution of the enriched component. However, these rocks are depleted in many lithophile elements (Ti, Zr, etc.).

Igneous rock assemblages in riftogenic systems of Phanerozoic folded domains. The temporal ε_{Nd} variation reveals an evolutionary trend. Data on the Russian sector of the Pacific Ocean–continent transitional foldbelt show that the contribution of depleted material decreases and the involvement of enriched material increases from the older (Cretaceous) to younger (Cenozoic) igneous rocks in the following sequence (figure): volcanics of back-arc riftogenic structures with ε_{Nd} values ranging from +5.0 to +11.9, volcanics of rif-

Karpinskii All-Russia Research Institute of Geology (VSEGEI), Srednii pr. 74, St. Petersburg, 199026 Russia